Primary Beam Corrections of MeerKAT Getting it Right

W. D. Cotton (NRAO), M. de Villiers (SARAO) draft February 26, 2024

***Abstract*—Alt-Az mounted radio antennas always have beam asymmetries which can cause imaging artifacts in interferometer arrays when these asymmetries cause variable gain in a given direction on the sky. If the detailed beam shape is known, it can, in principle, be corrected. This memo explores making beam corrections to reference pointed MeerKAT data. A comparison between the measured beam holography and a strong, weakly polarized calibrator viewed in a number of off–axis positions is presented. The beam images can be used to model the variations in the baseline averaged flux density with parallactic angle and applying them in the imaging process reduces, but does not eliminate, the level of artifacts, especially for Stokes Q and U. These residual artifacts can be explained by additional gain effects not included in the correction by the antenna average beam pattern. Antenna-to antenna variations in the beam are a possible cause.**

***Index Terms*—Primary Beam Correction, Interoferometric Synthesis**

I. Introduction

THE dynamic range of images made with interferometer arrays can be limited by artifacts resulting from bright, off-axis sources being observed with antennas whose gain is a function of time with alt-az mounted antennas. These gain variations can arise from a number of effects including antenna mechanical mispointing and azimuthal asymmetries in the antenna gain pattern. Pointing errors can be greatly reduced using referenced pointing but antenna pattern effects need to be corrected during imaging using knowledge of the beam pattern.

Attempts to correct VLA data using holographically measured antenna patterns with varying degrees of success are reported in [1], [2]. The technique used in this memo is verified using simulated data as described in [3], [4], [5].

This memo describes an attempt to apply primary beam corrections using the Obit [6][1] package to reference pointed MeerKAT L band data and follows the efforts in [7]. The holographically measured beam pattern of [8], [9] is used. The beam patterns used have been normalized such that the central pixel in the real parts of the parallel hand beam are essentially 1.0.

II. 14 June 2023 Reference Pointing Test

A test of reference pointing with MeerKAT at L band was performed on 14 June 2023 using the bright weakly polarized calibrator PKS0408-65. The observations occurred over 4 hours and antenna pointing errors were determined and corrected every 20 min. Cyclical observations were made with the calibrator on–axis and offset in the 4 cardinal directions, the pointing centers are given in Table I. The observations also included two scans on the polarized calibrator 3C138 (J0521+1638). The data were calibrated as described in [10]. For initial testing only Stokes I and no conversion to a circular basis was used. The data were divided into 8 Spectral windows (AKA IFs) for calibration purposes. Testing used phase self-calibrated data. In the nomenclature used the horizontal (H) feeds are referred to as "X" and the vertical (V) feeds as "Y".

TABLE I
14 June 2023 Pointing Offsets

Pointing	δRA °	δDec °
0408-65	0.0	0.0
J0400-6544	0.833433	-0.0133006
J0408-6635	0.0	0.8332818
J0416-6544	-0.833383	-0.0132995
J0408-6455	0.0	-0.8332472

The expectation is that the variations in antenna gain in the direction of PKS0408-65 in the offset positions is due to the variation of antenna gain with parallactic angle with time. It is also assumed that, after pointing corrections, all antennas will have approximately the same beam pattern. This expectation can be tested by comparing the observed visibilities with the average L band beam of [9].

A. Averaged Visibility Gains

One method of estimating the antenna gain in each correlation product (XX,YY,XY,YX) gains is to average the data over baseline and normalize by the total intensity as a function of frequency. The technique for averaging over baseline with a shift in phase tracking center is described in [11] and is implemented in ObitTask AvgBL. The various offset pointings averaged over baseline and in 30 second segments and normalized by the total Stokes I flux density of PKS0408-65 for channel 40 of Spectral window (IF) 8 are shown in Figure 1. The solid line is an estimate derived from knowledge of the observing geometry to determiine the track through the antenna patterns and the flux density of the source

National Radio Astronomy Observatory, 520 Edgemont Rd., Charlottesville, VA, 22903 USA email: bcotton@nrao.edu

[1]http://www.cv.nrao.edu/∼bcotton/Obit.html

on axis. Since all the offsets are the same distance from the center of the beam it is possible to plot all data on the same plot using parallactic angle to indicate the orientation in the beam of the offset point. Figure 1 shows excellent agreement between the data averages and the simplistic model based on the beam images.

B. Source Response to Beam Pattern

The beam images are the measured complex voltage patterns in a cube of frequency planes. The various beam images collectively define the Jones matrices for each pixel in each frequency plane. The expected visibility as a 2×2 complex matrix is the source flux density (s) times the Jones matrix at one end of the baseline times the complex transpose of the Jones matrix at the other end:

$$Vis_{Beam} \;=\; J_1 \; s \; J_2^{*T}$$

In the present case, all antennas are assumed to have the same beams.

The expected model visibility for an unpolarized point source can be derived from the holography beam images by:

$$\begin{pmatrix} XX_{Beam} & XY_{Beam} \\ YX_{Beam} & YY_{Beam} \end{pmatrix} = \\ I \begin{pmatrix} B_{XX}\ B_{XX}^* + B_{YX}\ B_{YX}^* & B_{XY}\ B_{YY}^* + B_{XX}\ B_{YX}^* \\ B_{YY}\ B_{XY}^* + B_{YX}\ B_{XX}^* & B_{YY}\ B_{YY}^* + B_{XY}\ B_{XY}^* \end{pmatrix}$$

where I is the total intensity, B_{XX}, B_{XY}, B_{YX} and B_{YY} are the complex beam responses in XX, XY, YX and YY interpolated at the frequency and the corresponding beam location. Note, the original beam images are upside down and labeled with X and Y swapped from the Obit usage.

Measured visibilities on the offset pointings on 0408-65 normalized by the on axis total flux density are plotted in Figure 1 for a single channel towards the top of the band. The data are averaged over baseline and to one half minute. The corresponding visibilities expected from the beam patterns and the on–axis flux density are shown as solid lines. The beam pattern is shown to closely reproduce the measurements. The imaginary part of the parallel hand measurements are residual calibration errors.

C. UVPolCor

The ultimate goal is to use the beam patterns to make corrections during imaging. A step in this direction is using task UVPolCor which calculates the actual response to a Stokes I sky model. Stokes I images of the various pointing offsets were made using no beam corrections and then used in UVPolCor to estimate the model visibilities. These visibilities were averaged and plotted as was described for the visibilities in Section II-A and plotted in Figure 2.

UVPolCor calculates model visibilities that would have been observed with perfect antenna patterns with the same shape as is assumed for the MeerKAT antennas[2]. This ratio of real to symmetric gain corresponding to Figure 2 is shown in Figure 3. Figure 4 is a version of Figure 2 with the model shown as a line corrected for the gain ratio in Figure 3. This explains some, but not all, of the difference between the two model estimates in Figure 2.

[2]In this meaning, the "perfect" antenna pattern is a circularly symmetric, cosine beam, which has no mixing between Stokes parameters.

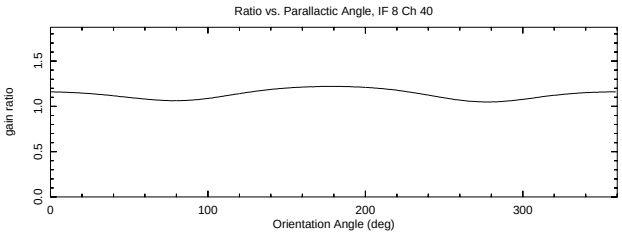

Fig. 3. The ratio of the beam pattern Stokes I response to the assumed symmetric beam pattern for IF 8 channel 40 at the offset used in these observations as a function of parallactic angle.

The difference between the two models shown in Figures 2 and 4 is that the points represented by *s were derived using the CLEAN components from a CLEAN with no correction for the beam effects and the line was from a point model of the known flux density and location in the beam. The *s will therefore include the effects of the errors in the imaging as well as the other sources in the field. Note: this point also applies to Figure 1. The averaging over baseline essentially creates a single pixel dirty image of the data which reduces the direct response of other sources but not their sidelobes.

1) Residual Visibilities: The residuals of the model from UVPolCor shown in Figure 2 are shown in Figure 5 as *s with the idealized model for reference.

D. MFBeam

The end goal of this exercize is to incorporate the beam corrections into the imaging. This is done in task MFBeam which is designed to use one or more sets of beam images in the deconvolution process. The region around 0408-65 from each of the offset pointing datasets was imaged with beam corrections in MFBeam. The imaging used a CLEAN mask restricted to within a radius of 4 pixels around 0408-65 and in boxes around other sources in the field. Since 0408-65 is so weakly polarized only Stokes I was deconvolved and only dirty images were made of Stokes Q, U and V. To show the residual artifacts, the CLEAN components were not restored. The CLEANing proceeded slowly, each major cycle was stopped when the peak residual reached 75% of the initial peak. Cleaning proceeded for 500 components or a minimum flux density of 1 mJy/bm with a loop gain of 0.1. To provide a comparison, MFImage was used in the same mode but without beam corrections. A comparison of the broadband results is shown in Figures 6 - 9.

One measure of how well the beam correction technique is working is the variation in the peak brightness of a given source offset from the pointing as it rotates with parallactic angle through the antenna pattern. Uncorrected, the peak brightness will vary with orientation within the beam due to the asymmetries in the beam pattern. With perfect correction the peak brightness will be constant. The process used in

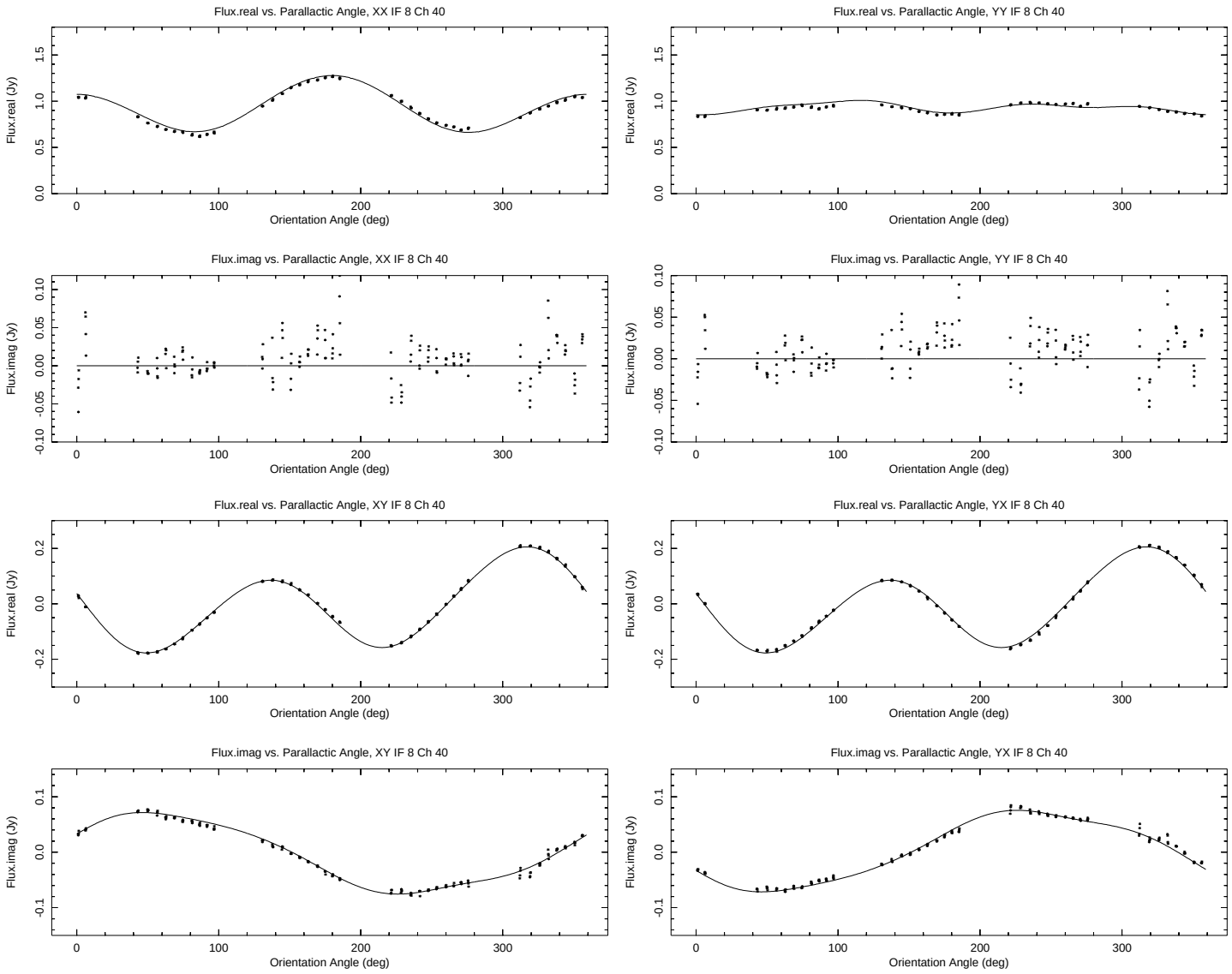

Fig. 1. Normalized visibilities of the various offset pointings of 0408-65 ("+") shown as a function of orientation in the beam of IF 8 channel 40. The solid line is the corresponding component of the product of the Jones matrix representation the antenna beam model interpolated to the corresponding beam location and frequency multiplied by the on–axis flux density.
Top Left: XX
Top Right: YY
Bottom Left: XY
Bottom Right: YX

MFBeam should convert the data to what would have been observed had the beam pattern been symmetric. Both MFImage and MFBeam report the peak brightness at the completion of deconvolution based in the sum of CLEAN component flux densities within a couple pixels of the peak. These values for the four pointing offsets are given in Table II. The fractional peak–to–valley variation for MFImage (no correction) is 0.26 and for MFBeam is 0.09; MFBeam gives a result much closer to the ideal than MFImage.

E. Other Gain Effects

Figures 6 - 9 show the residual images around 0408-65 with standard calibration and corrections for the average antenna pattern but artifacts remain. To determine if these residual artifacts are due to antenna based gain effects, an amplitude and phase self calibration was applied after imaging with beam corrections. This allows antenna specific gain effects to be identified. The resultant images are compared with only beam corrected images in Figure 10. Amplitude and phase self calibration signifigantly reduces the level of artifact indicating that they are due to gain effects not included in the beam corrections.

III. 3C286 AT L BAND

The previous examples have all been of an unpolarized source. Ben Hugo kindly provided observations of the strongly

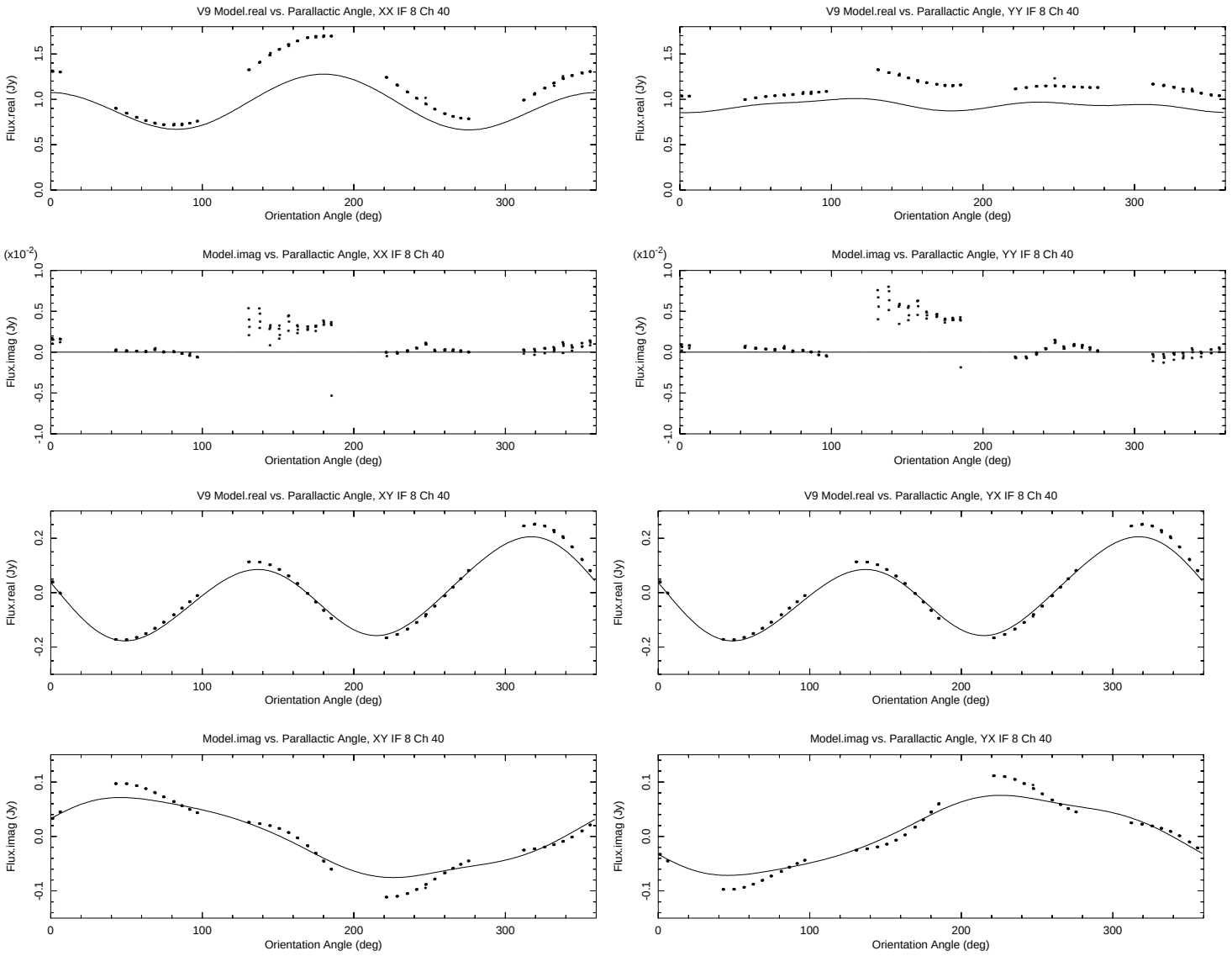

Fig. 2. Visibilities estimated by task UVPolCor of the various offset pointings of 0408-65 ("+") shown as a function of orientation in the beam of IF 8 channel 40.
The solid line is the corresponding component of the product of the Jones matrix representation the antenna beam model interpolated to the corresponding beam location and frequency times the on–axis flux density.
Top Left: XX
Top Right: YY
Bottom Left: XY
Bottom Right: YX

polarized source 3C286. This data is plotted as points and the model from his polarization model of 3C286 and the beam model is given in Figure 11. The flux density (s) at frequency ν (in MHz)

$$x_\nu = \log_{10}(\nu); c_a = 1.480; c_b = 0.292; c_c = -0.124$$

$$f = c_a + c_b\ x_\nu\ +\ c_c\ x_{nu}^2$$

$$\mathrm{s} = 10^f$$

If λ is the wavelength (in m) corresponding to ν then the EVPA (χ in deg) [12]) is

$$\chi\ =\ 32.64 + 85.37\lambda^2; \quad \nu > 1.7\ \mathrm{GHz}$$

$$\chi\ =\ 29.53\ +\ \lambda^2\ 4005.88\ x_\nu^3 - 39.38; \quad \text{otherwise.}$$

The fractional polarization (f_{pol}) is

$$f_{pol} = 0.080 - 0.053\ \lambda^2 - 0.015\ \log_{10}(\lambda^2); \quad \nu > 1.1\ \mathrm{GHz}$$

$$f_{pol} = 0.029 - 0.172\ \lambda^2 - 0.067\ \log_{10}(\lambda^2) \quad \text{otherwise.}$$

IV. Beam correction applied to older data

In order to test if the beam corrections can usefully be applied to the older MeerKAT data, i.e. without offset pointing, the L band observation of Abell 3395 (AKA J0627.2-5428) from 15 March 2019 ([13]) were imaged in MFBeam and MFImage to compare the results with and without beam

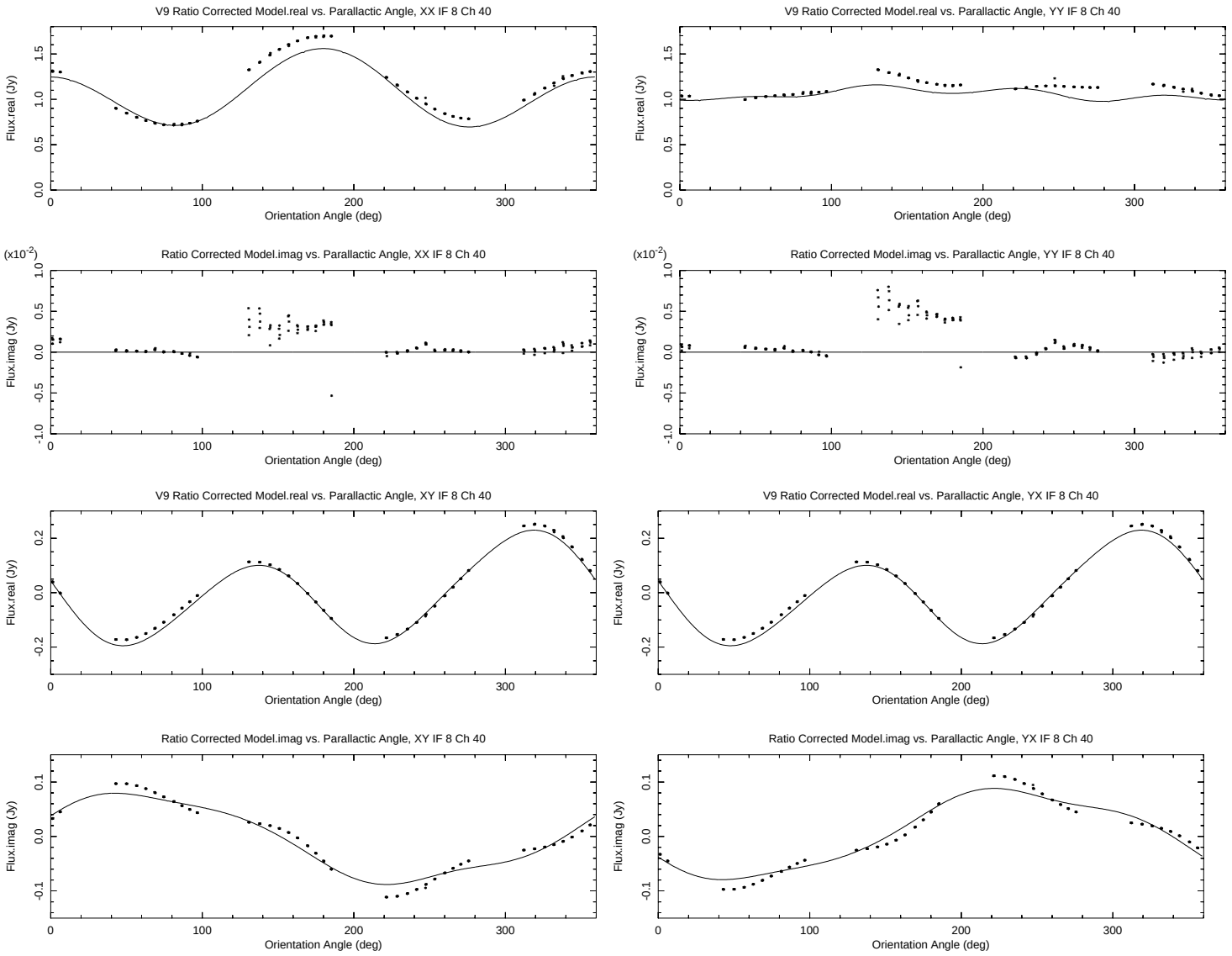

Fig. 4. Like Figure 2 but correcting the model shown as the line by the gain ratio shown in Figure 3.

TABLE II
14 JUNE 2023 PEAK STOKES I FLUX DENSITY

Pointing	MFImage	MFBeam
J0400-6544	2.55	2.07
J0408-6635	2.14	1.89
J0416-6544	2.30	1.96
J0408-6455	1.97	2.05

corrections. This field contains a strong, and likely polarized, AGN $\sim 0.8^\circ$ from the pointing center suitable for determining the effects of beam correction.

This data, from 2019, has relatively poor pointing characteristics. Two antennas in particular, m003 and m026 had particularly bad pointing and were flagged before imaging. Pointing errors of order 1 to 2 arcmin, as determined at other epochs, were common.

Images around the offset source in Stokes I, Q, U and V are shown in Figure 12. Stokes I and V are barely affected in this test. For Stokes Q and U, the extended, apparenty polarized regions are greatly reduced, as expected if they're due to off axis instrumental polarization. However, the fine scale artifacts near, but not on the Stokes I emission are more prominent in the "corrected" Q and U images. These fine scale artifacts may be due to residual pointing errors. The utility of this correction is unclear.

V. DISCUSSION

The ultimate test of the beam correction is the results shown in Figures 6 - 9. In all cases the level of artifacts around the offset pointings on 0408-65 are reduced relative making no beam corrections but some level of artifact remain. This improvement is most noticible in Stokes Q and U. Table II shows a greatly reduced variation of the peak brightness of

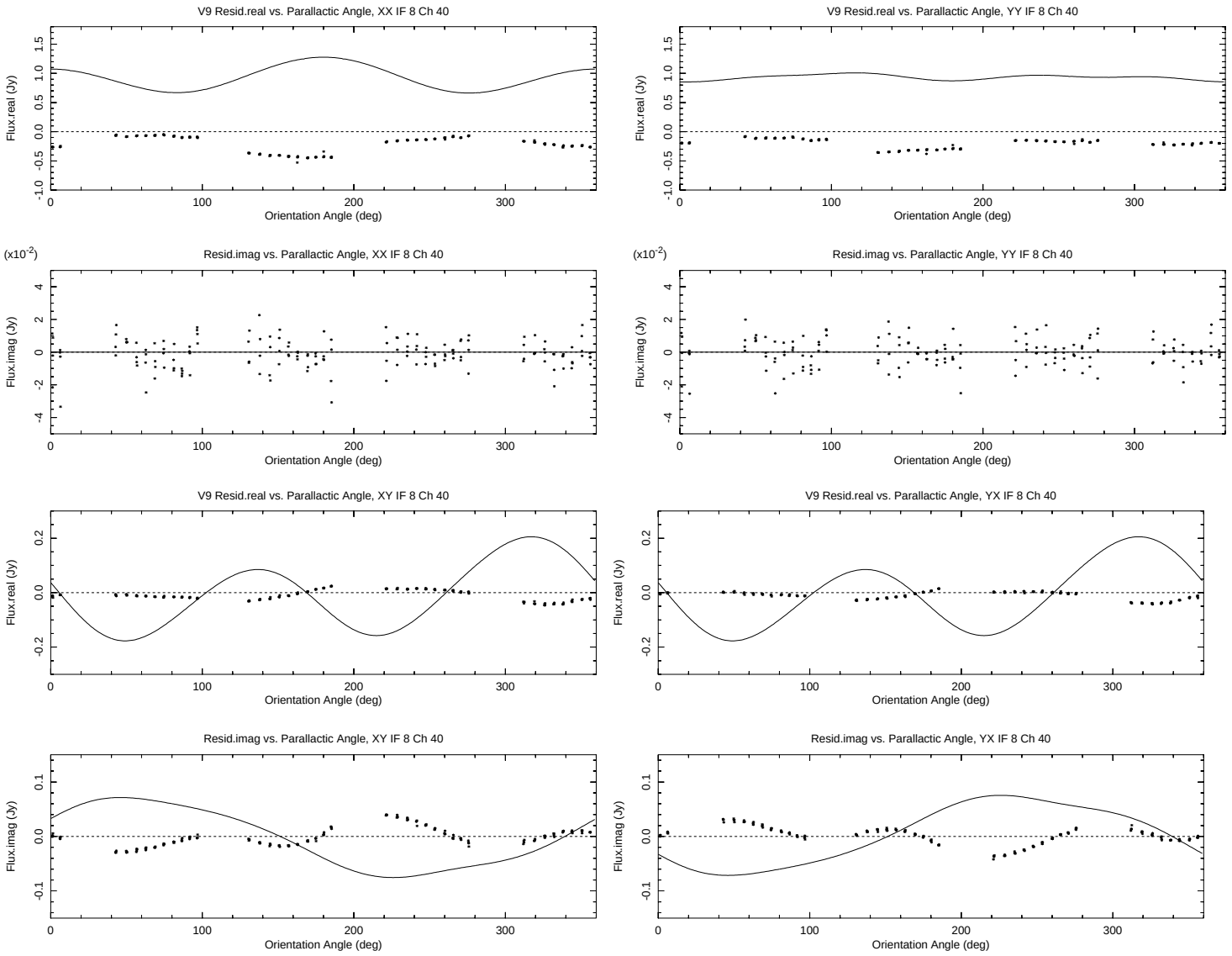

Fig. 5. Like Figure 2 but residuals of the model subtracted from the observed values as shown as *s. The solid lins are the idealized model as shown in FIgure 2. The dashed lines are at the zero level.

0408-65 with orientation in the antenna pattern at which it is observed. As expected, application of MFBeam results in a more nearly symmetric response to the strong offset source than the actual beam pattern. Amplitude and phase self cal following and initial imaging using MFBeam further reduces the residual artifacts. This is suggestive of antenna to antenna variations in the antenna pattern.

VI. Acknowledgment

We would like to thank the South African Radio Astronomy Observatory (SARAO) for access to the reference point test data and especially to Ludwig Swardt and Tom Mauch for making the observations and adjustments to the software. We also thank Ben Hugo for the 3C286 data.

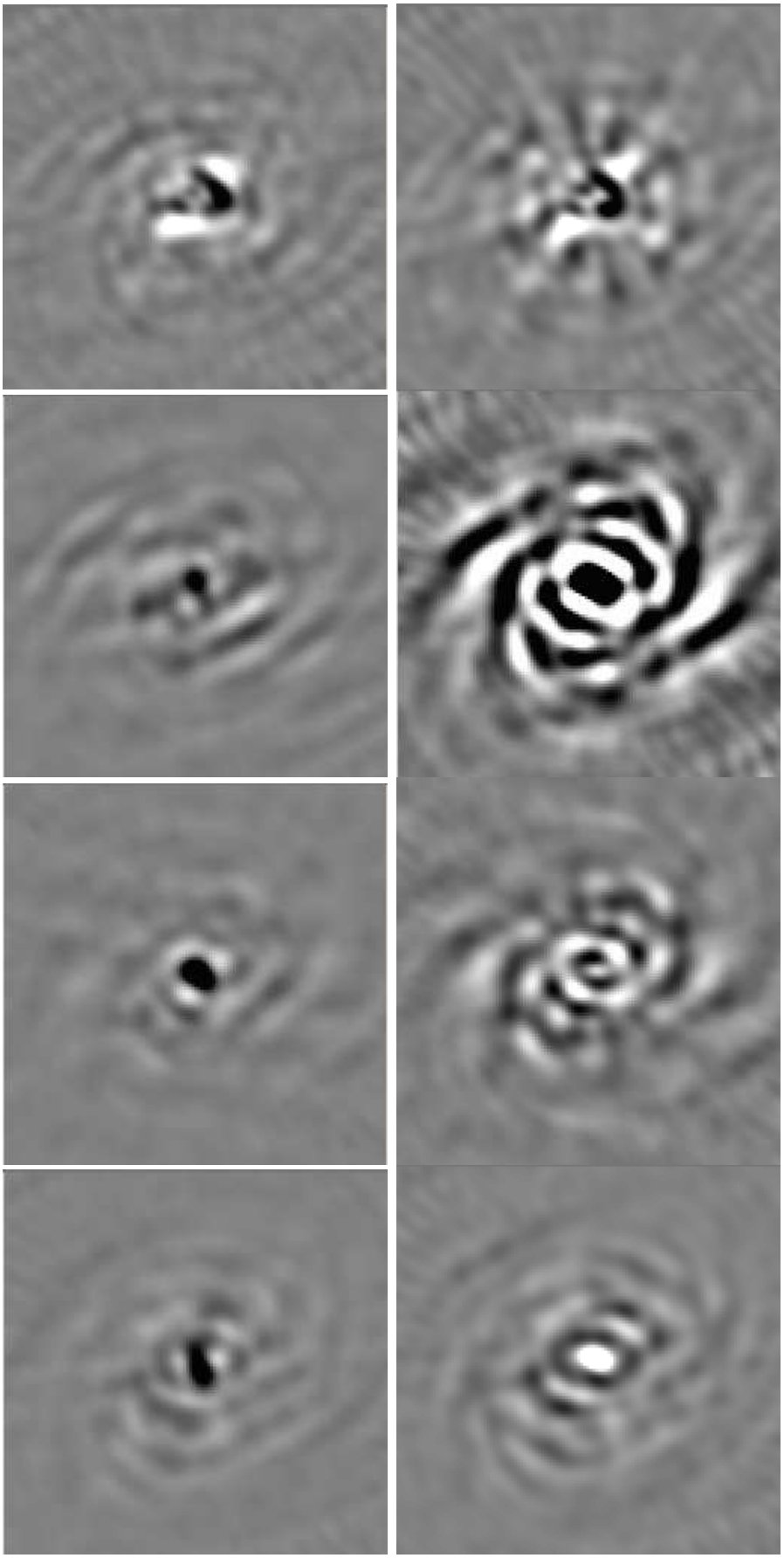

Fig. 6. J0400-6544: Broadband images around the position of 0408-65, left column with beam correction made, right column without. Each image is ± 80" centered on 0408-65.
Top Row: Stokes I residual, pixel range is ±5 mJy/beam.
Second Row: Stokes Q, pixel range is ±3 mJy/beam.
Third Row: Stokes U, pixel range is ±3 mJy/beam.
Botton Row: Stokes V, pixel range is ±3 mJy/beam.

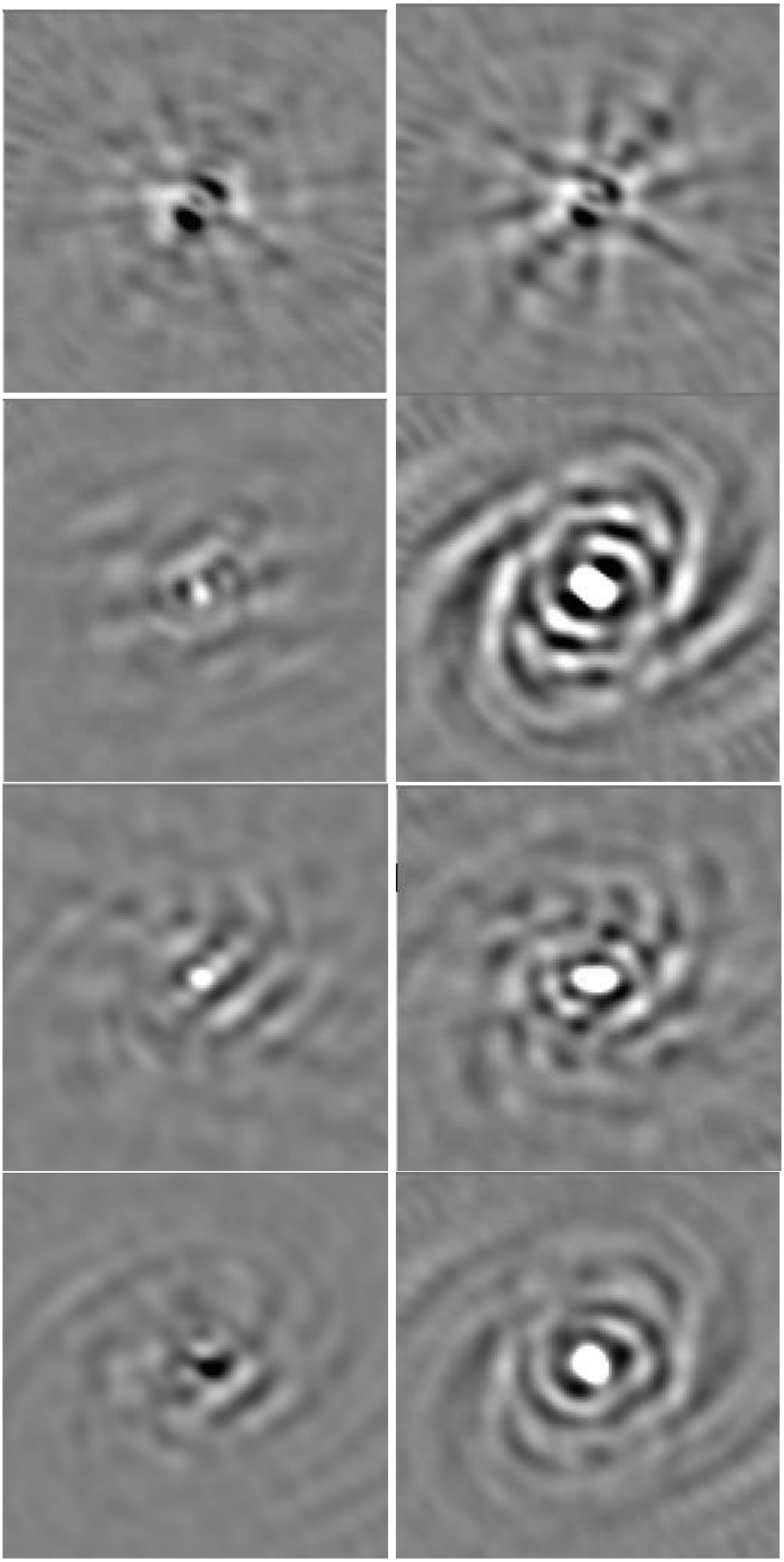

Fig. 7. Like Figure 6 but pointing J0408-6455.

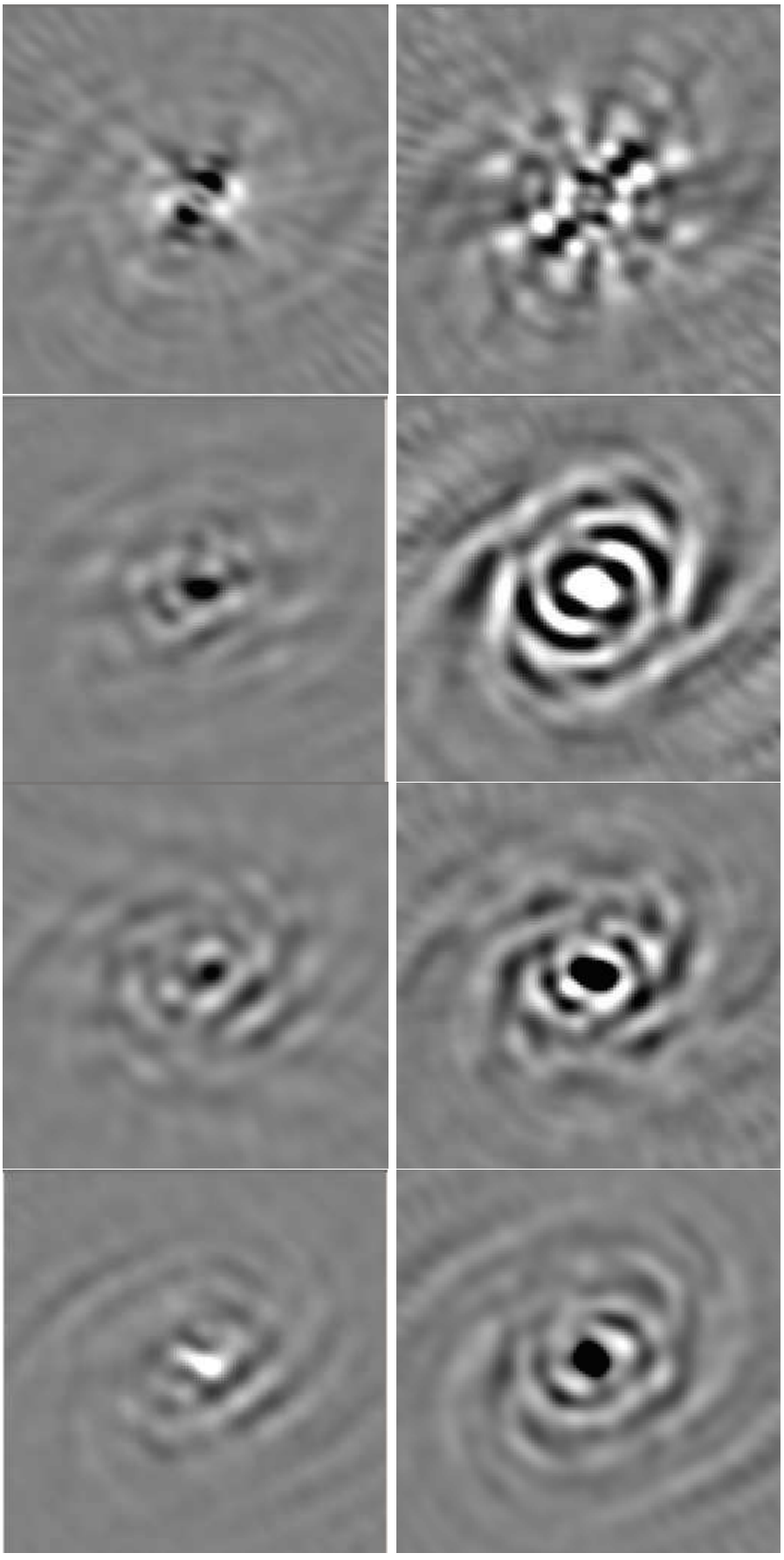

Fig. 8. Like Figure 6 but pointing J0408-6635.

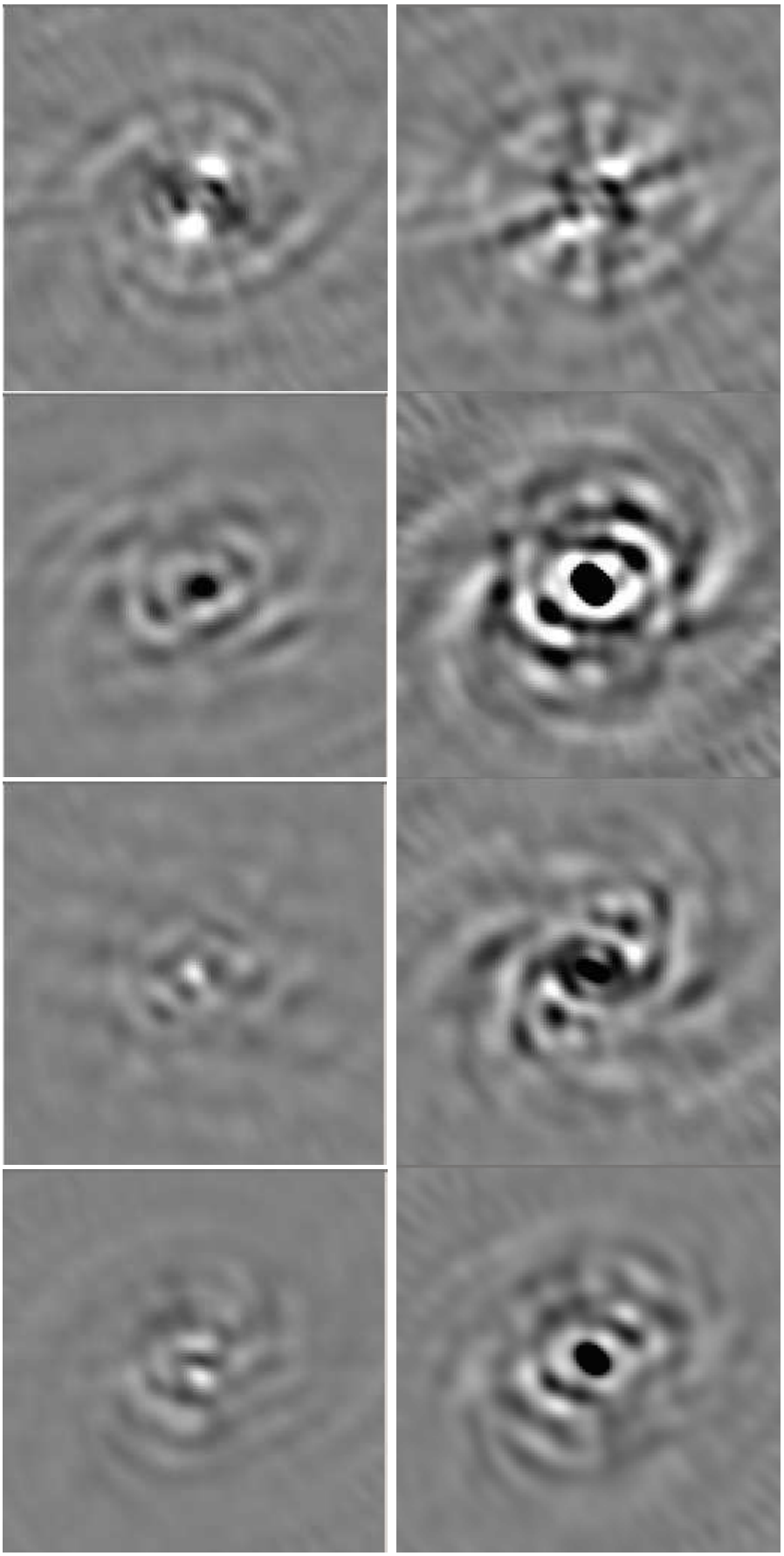

Fig. 9. Like Figure 6 but pointing J0416-6544.

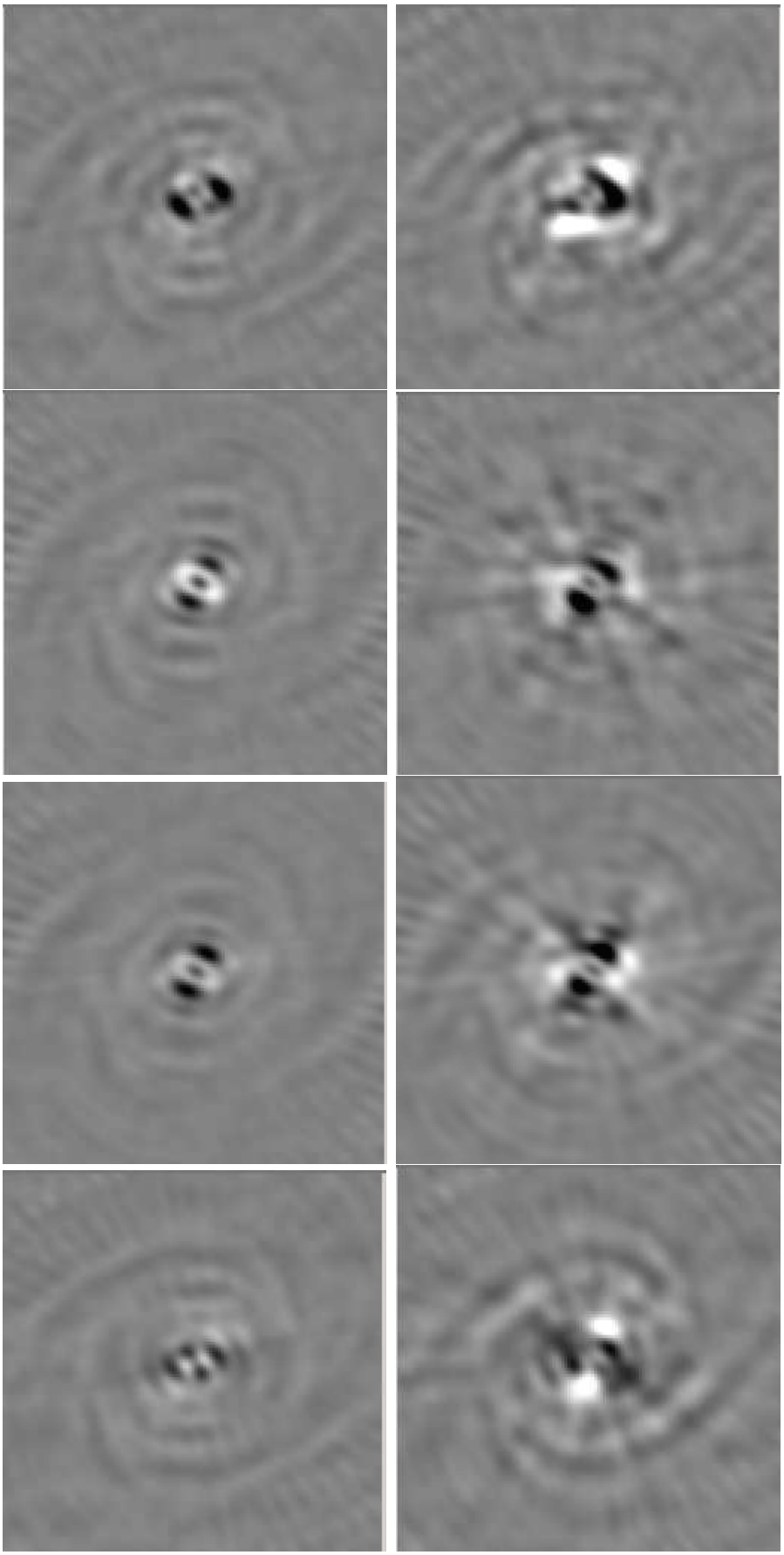

Fig. 10. Comparison of broadband Stokes I image residuals around the position of 0408-65 with beam corrections and self calibration. Left column images are following amplitude and phase selfcalibration; right column images have only beam corrections.
Top Row: J0400-6544
Second Row: J0408-6455
Third Row: J0408-6635
Bottom Row: J0416-6544
Each image is $\pm$ 80" centered on 0408-65.

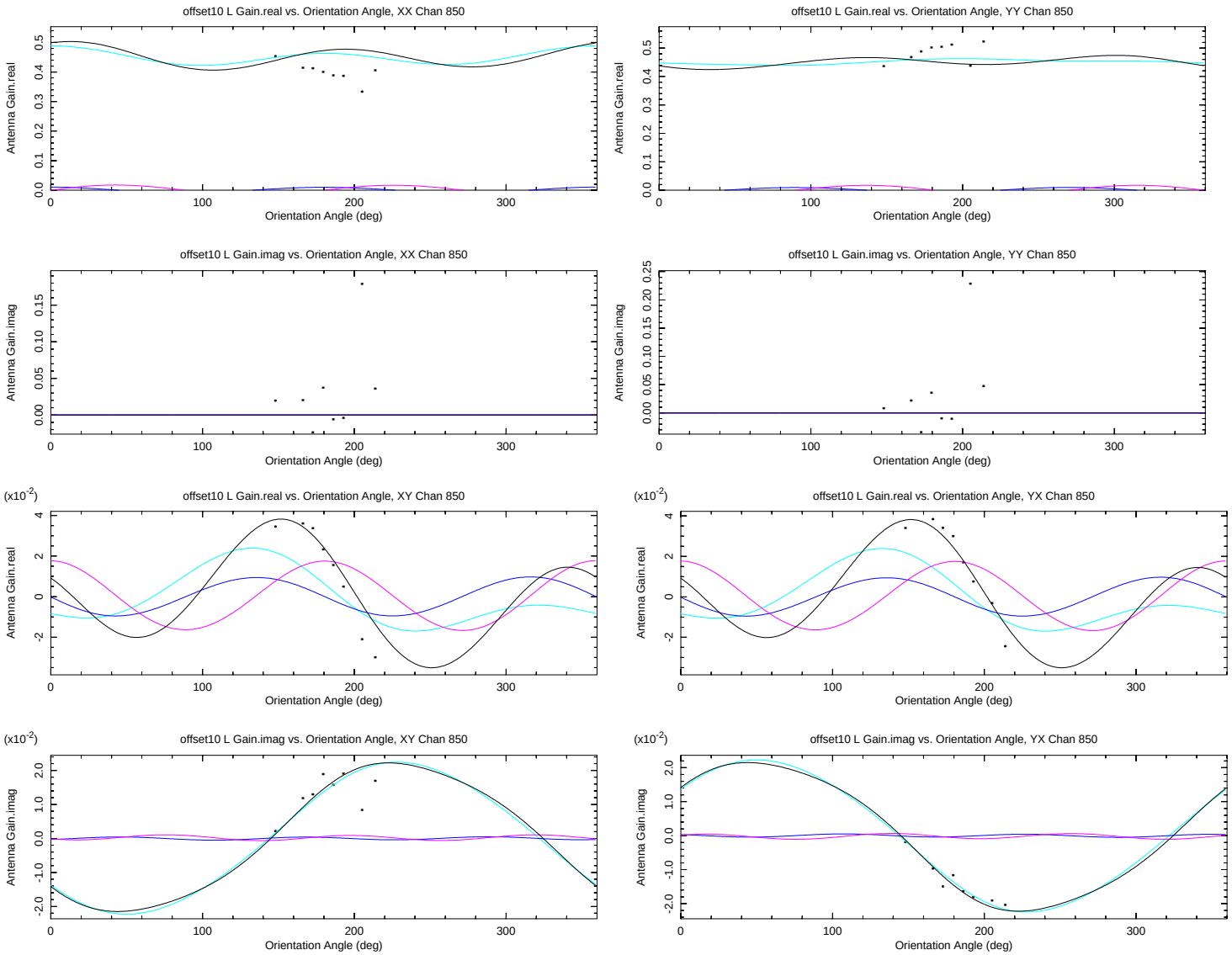

Fig. 11. Like Figure 2 but for 3C286 at L band offset from the pointing center by 0.5°. Line colors indicate the Stokes parameter of the contribution from the polarization model; cyan=Stokes I, blue=Q, magenta=U and black is the total.

REFERENCES

[1] W. D. Cotton and R. Perley, "EVLA Off-axis Beam and Instrumental Polarization," *Obit Development Memo Series*, vol. 17, pp. 1–22, 2010. [Online]. Available: https://www.cv.nrao.edu/∼bcotton/ObitDoc/EVLABeam.pdf

[2] ——, "EVLA Beam Holography take 2," *Obit Development Memo Series*, vol. 47, pp. 1–13, 2017. [Online]. Available: https://www.cv.nrao.edu/∼bcotton/ObitDoc/EVLABeam17.pdf

[3] W. D. Cotton and T. Mauch, "Beam Corrections and Heterogeneous Arrays I: Total Intensity," *Obit Development Memo Series*, vol. 70, pp. 1–, 2020. [Online]. Available: https://www.cv.nrao.edu/∼bcotton/ObitDoc/HeteroArray.pdf

[4] ——, "Beam Corrections and Heterogeneous Arrays II: Polarization," *Obit Development Memo Series*, vol. 71, pp. 1–, 2021. [Online]. Available: https://www.cv.nrao.edu/∼bcotton/ObitDoc/HeteroArrayPol.pdf

[5] ——, "Correction of Radio Interferometric Imaging for Antenna Patterns," *PASP*, vol. 133, no. 1028, p. 104502, Oct. 2021.

[6] W. D. Cotton, "Obit: A Development Environment for Astronomical Algorithms," *PASP*, vol. 120, pp. 439–448, 2008.

[7] ——, "Primary Beam Corrections of MeerKAT Reference Pointed Data," *Obit Development Memo Series*, vol. 80, pp. 1–11, 2023. [Online]. Available: https://www.cv.nrao.edu/∼bcotton/ObitDoc/MK_BeamCor.pdf

[8] M. S. de Villiers and W. D. Cotton, "MeerKAT Primary-beam Measurements in the L Band," *AJ*, vol. 163, no. 3, p. 135, Mar. 2022.

[9] M. S. de Villiers, "MeerKAT Holography Measurements in the UHF, L, and S Bands," *AJ*, vol. 165, no. 3, p. 78, Mar. 2023.

[10] J. J. Condon, W. D. Cotton, S. V. White, S. Legodi, S. Goedhart, K. McAlpine, S. M. Ratcliffe, and F. Camilo, "Threads, Ribbons, and Rings in the Radio Galaxy IC 4296," *ApJ*, vol. 917, no. 1, p. 18, Aug. 2021.

[11] W. D. Cotton, "Averaging over Baseline with Position Shift," *Obit Development Memo Series*, vol. 78, pp. 1–2, 2023. [Online]. Available: https://www.cv.nrao.edu/∼bcotton/ObitDoc/AvgBL.pdf

[12] B. Hugo and R. Perley, "Absolute linear polarization angle calibration using planetary bodies for MeerKAT and JVLA at cm wavelengths," *SARAO*, vol. SSA-0004E-001, 2024.

[13] K. Knowles, W. D. Cotton, L. Rudnick, F. Camilo, S. Goedhart, R. Deane, M. Ramatsoku, M. F. Bietenholz, M. Brüggen, C. Button, H. Chen, J. O. Chibueze, T. E. Clarke, F. de Gasperin, R. Ianjamasimanana, G. I. G. Józsa, M. Hilton, K. C. Kesebonye, K. Kolokythas, R. C. Kraan-Korteweg, G. Lawrie, M. Lochner, S. I. Loubser, P. Marchegiani, N. Mhlahlo, K. Moodley, E. Murphy, B. Namumba, N. Oozeer, V. Parekh, D. S. Pillay, S. S. Passmoor, A. J. T. Ramaila, S. Ranchod, E. Retana-Montenegro, L. Sebokolodi, S. P. Sikhosana, O. Smirnov, K. Thorat, T. Venturi, T. D. Abbott, R. M. Adam, G. Adams, M. A. Aldera, E. F. Bauermeister, T. G. H. Bennett, W. A. Bode, D. H.

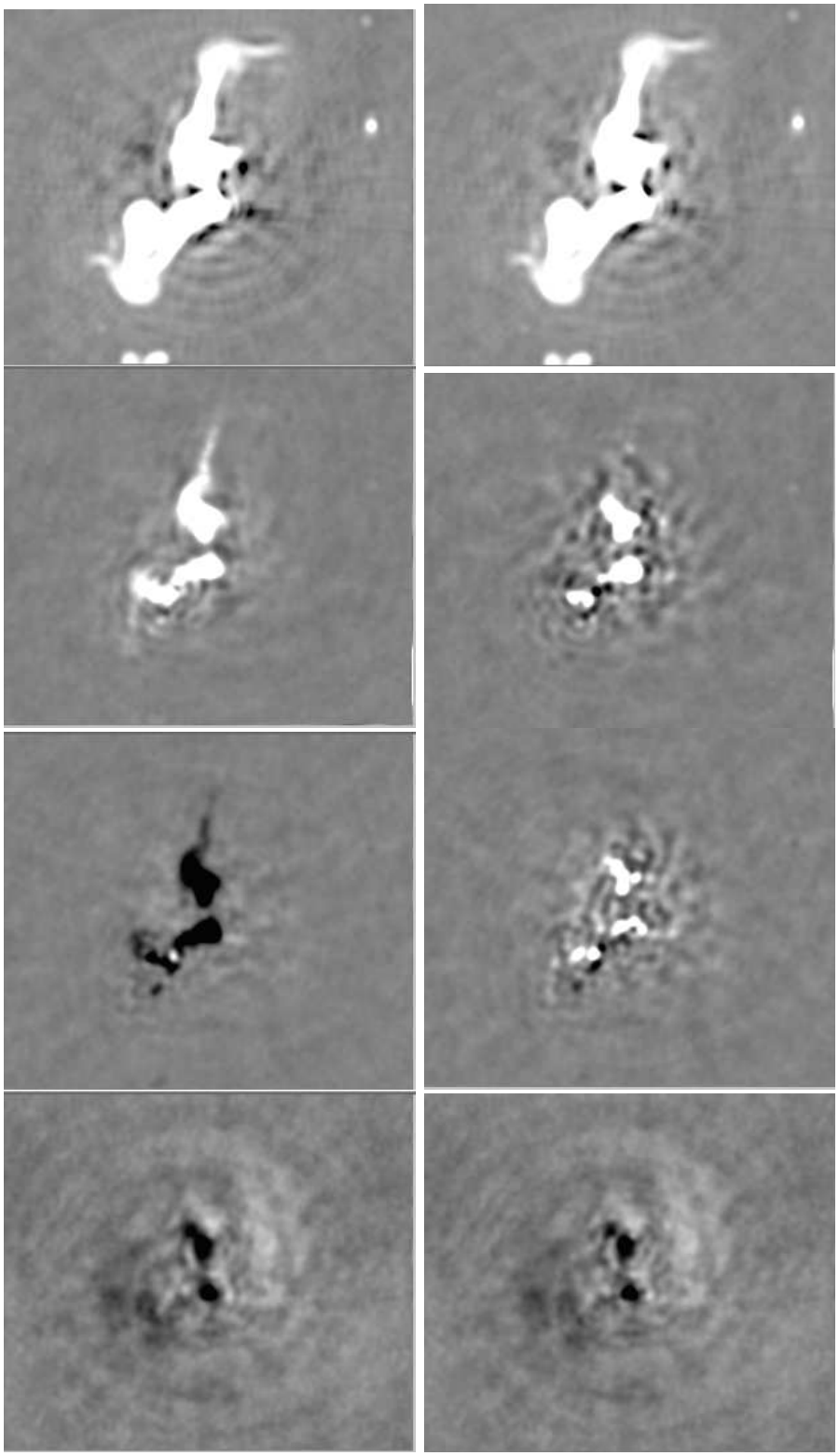

Fig. 12. Images of a source offset from the pointing in the Abell 3395 field. Left column images have no beam corrections right column images have beam corrections.
Top Row: I, Square root stretch -0.2 to 0.5 mJy/bm.
Second Row: Q, Linear stretch, $\pm$ 0.2 mJy/bm.
Third Row: U, Linear stretch, $\pm$ 0.2 mJy/bm.
Bottom Row: V, Linear stretch, $\pm$ 0.1 mJy/bm.
Each image is 6.4' $\times$ 5.6' centered on 06 26 20.92 -53 41 27.1.

Botha, A. G. Botha, L. R. S. Brederode, S. Buchner, J. P. Burger, T. Cheetham, D. I. L. de Villiers, M. A. Dikgale-Mahlakoana, L. J. du Toit, S. W. P. Esterhuyse, G. Fadana, B. L. Fanaroff, S. Fataar, A. R. Foley, D. J. Fourie, B. S. Frank, R. R. G. Gamatham, T. G. Gatsi, M. Geyer, M. Gouws, S. C. Gumede, I. Heywood, M. J. Hlakola, A. Hokwana, S. W. Hoosen, D. M. Horn, J. M. G. Horrell, B. V. Hugo, A. R. Isaacson, J. L. Jonas, J. D. B. Jordaan, A. F. Joubert, R. P. M. Julie, F. B. Kapp, V. A. Kasper, J. S. Kenyon, P. P. A. Kotzé, A. G. Kotze, N. Kriek, H. Kriel, V. K. Krishnan, T. W. Kusel, L. S. Legodi, R. Lehmensiek, D. Liebenberg, R. T. Lord, B. M. Lunsky, K. Madisa, L. G. Magnus, J. P. L. Main, A. Makhaba, S. Makhathini, J. A. Malan, J. R. Manley, S. J. Marais, M. D. J. Maree, A. Martens, T. Mauch, K. McAlpine, B. C. Merry, R. P. Millenaar, O. J. Mokone, T. E. Monama, M. C. Mphego, W. S. New, B. Ngcebetsha, K. J. Ngoasheng, M. T. Ockards, A. J. Otto, A. A. Patel, A. Peens-Hough, S. J. Perkins, N. M. Ramanujam, Z. R. Ramudzuli, S. M. Ratcliffe, R. Renil, A. Robyntjies, A. N. Rust, S. Salie, N. Sambu, C. T. G. Schollar, L. C. Schwardt, R. L. Schwartz, M. Serylak, R. Siebrits, S. K. Sirothia, M. Slabber, L. Sofeya, B. Taljaard, C. Tasse, A. J. Tiplady, O. Toruvanda, S. N. Twum, T. J. van Balla, A. van der Byl, C. van der Merwe, C. L. van Dyk, V. Van Tonder, R. Van Wyk, A. J. Venter, M. Venter, M. G. Welz, L. P. Williams, and B. Xaia, "The MeerKAT Galaxy Cluster Legacy Survey I. Survey Overview and Highlights," *A&A*, vol. 657, p. A56, Jan. 2022.